IEEE Access
Multidisciplinary : Rapid Review : Open Access Journal

Received March 29, 2022, accepted April 14, 2022, date of publication April 22, 2022, date of current version June 10, 2022.

Digital Object Identifier 10.1109/ACCESS.2022.3169750

Direct Thrust Force Control of Half-Open Winding Primary Permanent Magnet Linear Motor

QIANGGUO YU[1], WEI WANG[2], (Senior Member, IEEE), YANAN FENG[1], WEIJIE TIAN[2], (Graduate Student Member, IEEE), AND QING SHEN[1]

[1]School of Science and Engineering, Huzhou College, Huzhou, Zhejiang 313000, China
[2]School of Electrical Engineering, Southeast University, Nanjing, Jiangsu 210096, China

Corresponding author: Yanan Feng (fengyanan@zhjzu.edu.cn)

This work was supported by the National Natural Science Foundation of China under Project 61802123.

ABSTRACT In this paper, a direct thrust force control (DTFC) strategy is proposed for the half-open winding primary permanent magnet linear motor (PPMLM) drive system in order to improve the dynamic response and performance of flux weakening control. The independent voltage active vector (IVAV) is selected as the candidate voltage vector to suppresses the zero sequence current in the proposed DTFC (P-DTFC). Meanwhile, a new switch table is designed to determine the control vector while the complexity of control method is greatly simplified in P-DTFC. The simulation and experimental results verify that P-DTFC maintains better steady-state and dynamic-state performance with lower complexity compared with traditional DTFC (T-DTFC).

INDEX TERMS Open winding motor, direct thrust force control (DTFC), common mode voltage, zero sequence current, primary permanent magnet linear motor (PPMLM), independent voltage active vector (IVAV).

I. INTRODUCTION

Compared with the rotational motor traction system, the linear motor traction system has significant advantages [1]–[4]. Recently, permanent magnet linear motor (PMLM) has been paid great attentions for its light weight, smaller volume and higher power density [5]–[7]. However, the armature winding and PM material of conventional PMLM are always mounted on the mover or stator in which high cost and difficult maintenance must be needed in long distance application. Therefore, have proposed the primary permanent magnet linear motor (PPMLM) has been proposed, in which the PM materials and armature windings are all mounted on the mover (primary). The stator (secondary) is only composed of silicon steel sheets [8], [9]. As a result, the construction cost will be greatly reduced especially, when the PPMLM is applied in long-distance transportation system.

Considering the operation reliability of linear motor, its air gap is usually designed between 8 mm and 12 mm, which is longer than that of rotational motor [10], [11]. The increase of air gap inevitably lead to larger inductance which weakens the ability to modulate the magnetic field. Therefore, the magnetic field of PPMLM is usually adjusted by changing the flux weakening current while the copper loss is increased in this way.

Thinking of the demagnetization risk of PM and the working efficiency of traction system, open winding technology provides a more feasible scheme for PPMLM traction system. The neutral point of PPMLM is turned on in open winding electrical machine (OWEM) system. Meanwhile, two inverters are adopted for power supply which can double the output voltage of the system. In addition, the OWEM system also has strong fault tolerance [12]–[15] because of the topological characteristics of double power supply.

However, a loop path for zero sequence current is provided in the traditional OWEM system. Hence, a small zero sequence voltage component can contribute to large zero sequence current since the zero sequence impedance of the motor is very small [16], [17]. The zero sequence current can lead to copper loss and thrust force ripple. Therefore, the suppression of zero sequence current is significant for OWEM system [18]–[20].

The zero sequence current is generated by the zero sequence voltage of motor. Therefore, the zero sequence

The associate editor coordinating the review of this manuscript and approving it for publication was Ahmed A. Zaki Diab.

current can be suppressed by eliminating zero sequence voltage. The zero sequence voltage is usually divided into four parts: common mode voltage, third harmonic back electromotive force (EMF), dead time effect zero sequence voltage and $dq0$ coupled zero sequence voltage [21]. The proportion of dead time effect zero sequence voltage and $dq0$ coupled zero sequence voltage is always dismissed since they are small. As a result, most suppression methods only consider the common mode voltage and the third harmonic back EMF.

Based on the principle that the common mode voltage is zero, a specific voltage vector method is proposed in [22], and a periodic average zero sequence elimination method is proposed in [23], where the sum of common mode voltage during one duty cycle is zero.

It is obvious that the common mode voltage is determined by the output of the inverter while the other three zero sequence voltages are uncontrollable. Therefore, in order to further suppress the zero sequence voltage, several special modulation methods are adopted to generate particular common mode voltage to exactly counteract other zero sequence voltages [24]–[26]. The third harmonic component accounts for the largest proportion among the three components and several methods aims to suppress it [27], [28]. Model predictive control (MPC) is a model-based strategy which has rapid transient response [29]–[31]. MPC adopts cost function to evaluate each candidate vector instead of suppressing particular voltage component. However, one of fatal weakness of MPC is heavy computation cost since it needs to traverse all motor vectors.

Direct torque control (DTC) is based on hysteresis comparator which has good robustness and easy implementation. Therefore, the specific voltage vector method which will not lead into common mode voltage are used to cooperate with DTC to achieve good control performance [32]–[34].

Although the traditional OWEM system has many advantages, the number of power electronics devices will be doubled when the topology is adopted which increases the hardware cost and high system failure rate [35], [36]. In order to reduce the amount of power electronics devices for the OWEW traction system, a half open winding electrical motor (HOWEM) is proposed in this paper, which can reduce the number of power electronics devices from $2m$ to $m+1$ if a single m phase motor is applied in the OWEW systems. While the transformation cost and the additional weight can be significantly reduced. However, all these above-mentioned suppression methods of zero sequence current are proposed only for the OWEM system, the research of the HOWEM system is not be illustrated in any other papers or reports.

Thus, the HOWEM system is proposed in this paper, as shown in Figure 1. Compared to the OWEM system, the open winding operation of PPMLM traction system with less power electronics devices can be realized [37], [38]. Meanwhile, the direct thrust force control (DTFC) strategy is designed to suppress the zero sequence current. The proposed DTFC (P-DTFC) maintains the satisfactory steady-state and dynamic-state performance with less complexity.

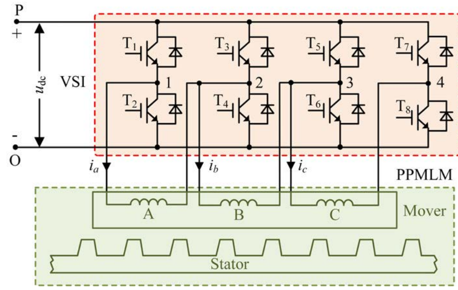

FIGURE 1. The topology of HOWEM system.

The paper is organized as follows. Firstly, the HOWEM system is characterized in Section II. Then in Section III, P-DTFC is introduced exhaustively and simulation analysis is implemented in Section IV. Next, the T-DTFC with the P-DTFC are compared by experimental results in Section V. In the final, some conclusions are inferred in Section VI.

II. STUDIED HOWEM SYSTEM

A. HOWEM SYSTEM TOPOLOGY

The studied HOWEM system is shown in Figure 1 in which a four-leg voltage source inverter (VSI) is adopted. As is illustrated in Figure 1, the bridge 2 and bridge 3 are connected with two-phase windings at the same time, which is called multiplex bridge. Meanwhile, the bridge 1 and bridge 4 are connected with only one phase winding, which is named as independent bridge. i_a, i_b and i_c are the motor phase current of PPMLM respectively, while u_{dc} is the DC-link voltage of PPMLM.

B. PPMLM

The structure of PPMLM and E-type module is exhibited in Figure 2 and Figure 3, respectively. The armature winding and PM materials are all mounted in the primary (mover) while the silicon steel sheets is only included in the secondary (stator). In the mover, the phase windings and different phases are all separated by magnetic barriers.

The dq axis of PPMLM is defined as demonstrated in Figure 4. The maximum position of phase-A PM flux linkage of PPMLM is d axis, and the q axis is 90° ahead of d axis (i.e. the front quarter stator pole pitch τ_s).

The voltage equation of PPMLM is expressed as:

$$\begin{cases} u_d = R_s i_d + L_s \dfrac{di_d}{dt} - \dfrac{2\pi v}{\tau_s} L_s i_q \\ u_q = R_s i_q + L_s \dfrac{di_q}{dt} + \dfrac{2\pi v}{\tau_s} (\psi_m + L_s i_d) \end{cases} \quad (1)$$

where u_d, u_q are dq-axis voltage, i_d, i_q are dq-axis current. R_s, L_s, ψ_m are stator resistance, inductance and PM flux linkage respectively. v is speed of mover. τ_s is the stator pole pitch.

III. PROPOSED DTFC

In this section, the P-DTFC is described in detail.

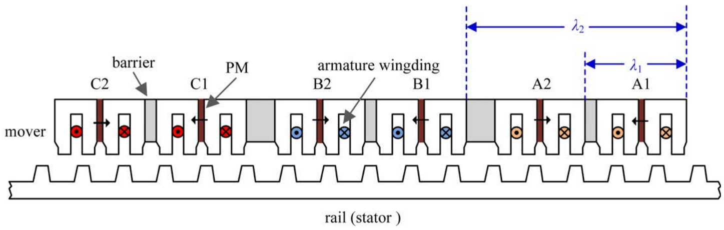

FIGURE 2. The structure of PPMLM.

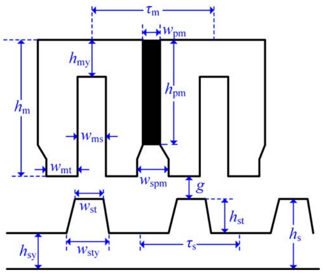

FIGURE 3. The structure of E-type module.

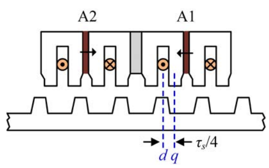

FIGURE 4. Definition of ***dq***-axis for PPMLM.

A. FORMATION PRINCIPLE OF ZERO SEQUENCE CURRENT

In HOWEM system, the zero sequence voltage equation can be formulated:

$$u_0 = e_0 + i_0 R_s + L_0 \frac{di_0}{dt} \tag{2}$$

where u_0, e_0, i_0, L_0 are zero sequence voltage, zero sequence induced voltage, zero sequence current and stator zero sequence inductance respectively. The zero sequence inductance L_0 is mainly leakage inductance which can be neglected. As a result, the i_0 can be large if u_0 and e_0 are not equal. The zero sequence voltage of HOWEM system is composed of four parts: common mode voltage, third harmonic back EMF, dead time effect zero sequence voltage and $dq0$ coupled zero sequence voltage. Since only the common mode voltage is controllable in the zero sequence voltage, this paper only analyzes the common mode voltage u_{com}, which is expressed as

$$u_{com} = \frac{1}{3}(u_a + u_b + u_c) \tag{3}$$

where u_{a}, u_{b} and u_{c} are phase voltage.

The switching state s_x of bridge x is defined as:

$$s_x = \begin{cases} 1 & \text{upper bridge is on} \\ 0 & \text{upper bridge is off} \end{cases} \quad (x = 1, 2, 3, 4) \tag{4}$$

The phase voltages can be derived from equation (4) as:

$$\begin{cases} u_a = u_{dc}(s_1 - s_2) \\ u_b = u_{dc}(s_2 - s_3) \\ u_c = u_{dc}(s_3 - s_4) \end{cases} \tag{5}$$

where u_{dc} is the DC-link voltage.

Substitute equation (5) into equation (3), u_{com} is presented as

$$u_{com} = \frac{1}{3} u_{dc}(s_1 - s_4) \tag{6}$$

It can be seen from equation (6) that the common mode voltage u_{com} is independent of the multiplexed bridge switching state (s_2, s_3) and only depends on the independent bridge switching state (s_1, s_4).

B. INDEPENDENT VOLTAGE ACTIVE VECTOR

Considering the different switch states, four-bridge has 16 voltage vectors which consist of 2 zero voltage vectors, 6 small voltage vectors, 6 medium voltage vectors and 2 large voltage vectors as shown in Figure 5. Small voltage vector and medium voltage vector can form a closed regular hexagon where the amplitude of medium voltage vector is two times that of small voltage vector. According to the previous analysis, the common mode voltage u_{com} is zero when zero voltage vector or medium voltage vector is implemented. Therefore, the medium voltage vector is defined as independent voltage active vector (IVAV) in this paper.

As mentioned above, the drive system can obtain high voltage utilization and zero common mode voltage if IVAV is adopted for VSI. Therefore, the IVAV is selected and numbered as the candidate voltage vector in this paper, as shown in Figure 5.

C. PROPOSED DTFC

Combined with the T-DTFC and the spatial distribution of IVAV, the P-DTFC based on HOWEM system is proposed in this section.

Voltage-integration-type flux observer is adopted as

$$\begin{cases} \boldsymbol{\psi}_\alpha = \int (\boldsymbol{u}_\alpha - R_s \boldsymbol{i}_\alpha) dt + \boldsymbol{\psi}_m \cos(\theta_{e0}) \\ \boldsymbol{\psi}_\beta = \int (\boldsymbol{u}_\beta - R_s \boldsymbol{i}_\beta) dt + \boldsymbol{\psi}_m \sin(\theta_{e0}) \end{cases} \tag{7}$$

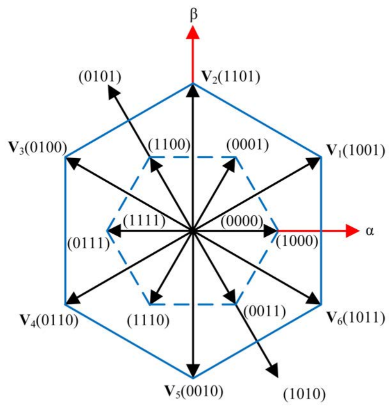

FIGURE 5. The space distribution of voltage vector.

where, i_α, i_β, u_α, u_β, ψ_α, ψ_β are current, voltage and flux linkage of PPMLM in synchronous coordinate system, while θ_{e0} is the initial electric angle of the mover.

The amplitude and angle of flux linkage are calculated by

$$\begin{cases} \psi_s = \sqrt{\psi_\alpha^2 + \psi_\beta^2} \\ \theta_s = \arctan(\psi_\beta/\psi_\alpha) \end{cases} \tag{8}$$

Thrust force F_e is expressed as

$$F_e = \frac{3\pi}{\tau_s}(\psi_\alpha i_\beta - \psi_\beta i_\alpha) \tag{9}$$

Different from the T-DTFC, the sector is redefined in this paper as is illustrated in Figure 6 and Table 1 since the spatial distribution of IVAV has changed.

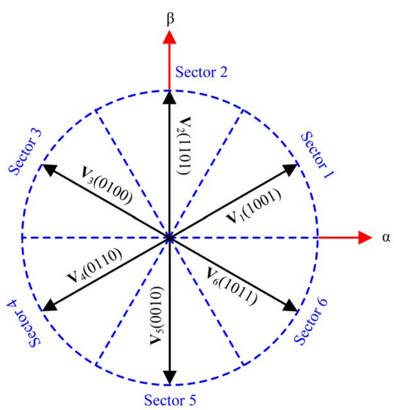

FIGURE 6. The space distribution of IVAV and sector.

According to flux linkage angle θ_s and Table 1, the sector N can be determined where the flux linkage is located. The hysteresis comparator is adopted to obtain the thrust force command σ_F and flux linkage commands σ_ψ by

$$\sigma_F = \begin{cases} 1 & (e_F > H_F) \\ 0 & (e_F < -H_F) \end{cases} \quad (e_F = F_e^* - F_e) \tag{10}$$

TABLE 1. The determination of flux sector ***N***.

Sector	θ_s	Sector	θ_s
Sector 1	[0,π/3)	Sector 4	[-π, -2π/3)
Sector 2	[π/3,2π/3)	Sector 5	[-2π/3,-π/3)
Sector 3	[2π/3,π)	Sector 6	[-π/3,0)

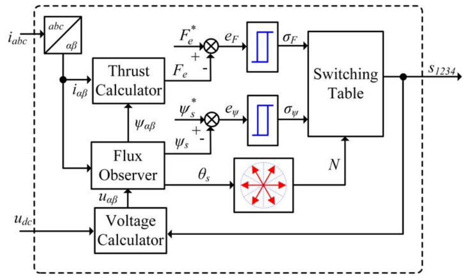

FIGURE 7. The control block diagram of P-DTFC.

TABLE 2. The selection principle of IVAV.

	σ_ψ=1		σ_ψ=0	
	σ_F=1	σ_F=0	σ_F=1	σ_F=0
Sector 1	V_2(1101)	V_6(1011)	V_3(0100)	V_5(0010)
Sector 2	V_3(0100)	V_1(1001)	V_4(0110)	V_6(1011)
Sector 3	V_4(0110)	V_2(1101)	V_5(0010)	V_1(1001)
Sector 4	V_5(0010)	V_3(0100)	V_6(1011)	V_2(1101)
Sector 5	V_6(1011)	V_4(0110)	V_1(1001)	V_3(0100)
Sector 6	V_1(1001)	V_5(0010)	V_2(1101)	V_4(0110)

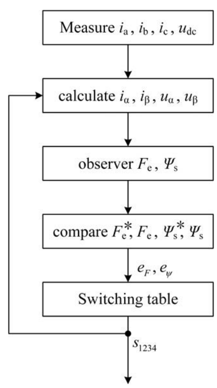

FIGURE 8. The flowchart diagram of P-DTFC.

$$\sigma_\psi = \begin{cases} 1 & (e_\psi > H_\psi) \\ 0 & (e_\psi < -H_\psi) \end{cases} \quad (e_\psi = \psi^* - \psi_s) \tag{11}$$

where H_F and H_ψ are the thrust force and flux linkage band width, respectively.

According to σ_F, σ_ψ and sector N, the IVAV is selected from Table 2 and implemented to the driving of PPMLM.

The P-DTFC block diagram is shown in Figure 7.

The flowchart diagram of P-DTFC is shown in Figure 8.

IV. PERFORMANCE ANALYSIS

To verify the feasibility of P-DTFC, several simulation experiments are carried on based on MATLAB in Section IV. The simulation parameter is listed in Table 3.

TABLE 3. The parameters of simulation.

Parameter	Value
DC-link voltage, u_{dc} (V)	50
Simulation step, T_s(s)	1E-6
Sampling period, T_{sc}(s)	5E-5
Stator inductance, L_s(mH)	32.5
Stator resistance, R_s(Ω)	3.3
PM flux linkage, ψ_s(Wb)	0.125
Rated thrust, F_e(N)	150
Friction coefficient, D(kg/s)	0.004
Mover mass, M(kg)	32.6

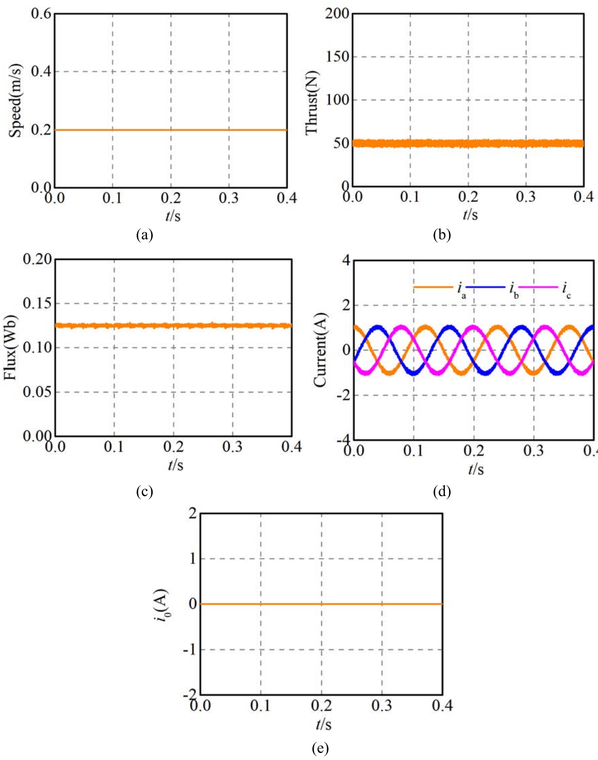

FIGURE 9. Steady-state simulation performance of P-DTFC: (a) speed, (b) thrust, (c) flux (d) phase current, (e) zero sequence current.

A. STEADY-STATE PERFORMANCE OF SIMULATION

To analyze the steady-state performance of the P-DTFC, the speed is set as 0.2 m/s and the load is set as 50 N. The simulation results are shown in Figure 9.

It can be found that the P-DTFC demonstrates good steady-state performance in which the speed and thrust force of PPMLM can track the reference value well. The sinusoidal degree of three-phase current is high with less harmonic content. Meanwhile, the zero sequence current is nearly zero, which is consistent with the previous analysis.

B. SPEED RESPONSE OF SIMULATION

To test the speed response simulation performance of the P-DTFC, the reference speed increases from 0.2 m/s to 0.4 m/s, then recovers to 0.2 m/s, while the load is set as 50 N. The simulation results are illustrated in Figure 10.

It is found that the speed tracks the reference value well, while the flux linkage can maintain a constant value despite

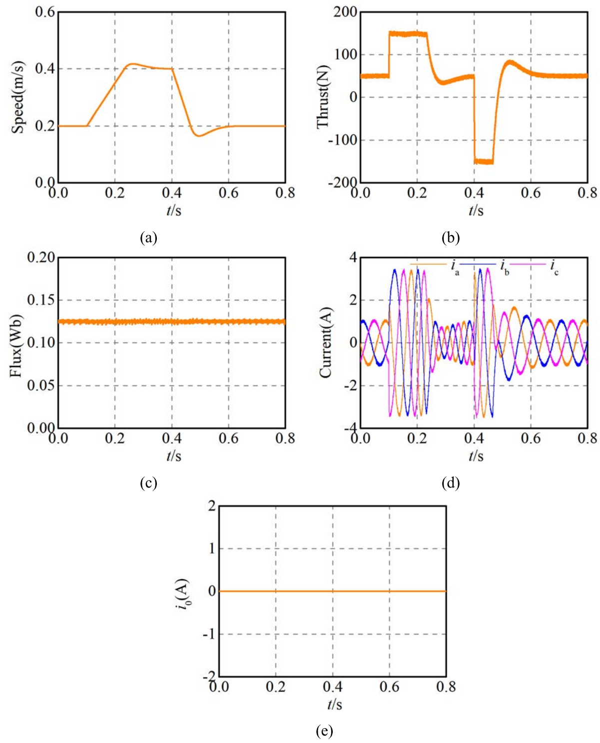

FIGURE 10. Speed response simulation performance of P-DTFC: (a) speed, (b) thrust, (c) flux (d) phase current, (e) zero sequence current.

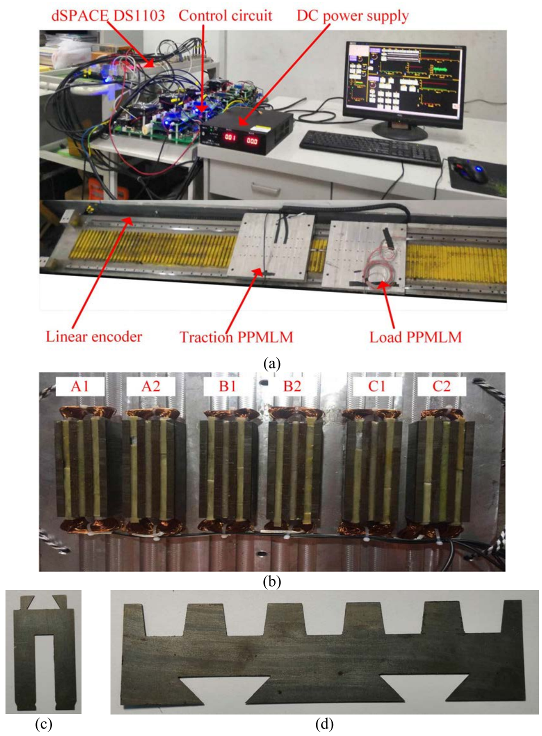

FIGURE 11. Experiment platform: (a) entire view, (b) bottom view of mover, (c) mover teeth (d) stator (rail) teeth.

the disturbance of speed, in line with the previous theoretical. Similarly, the zero sequence current can also be neglected in dynamic operation since only the medium voltage vector is adopted.

TABLE 4. The parameters of PPMLM.

Parameter	Value
Mover width, w_m (mm)	160
Mover pole pitch, τ_m (mm)	26
Stator pole pitch, τ_s (mm)	24
Mover tooth width, w_{mt} (mm)	τ_m/4
Mover slot mouth width, w_{msm}(mm)	τ_m/4
Mover slot width, w_{ms} (mm)	τ_m/4
Slot width (Under PM), w_{ms} (mm)	τ_m/4
Mover height, h_m (mm)	35
Mover yoke height, h_{my} (mm)	10
Magnet height, h_{pm} (mm)	0.9*h_m
Magnet width, w_{pm} (mm)	5
Air gap length, g (mm)	2
Stator tooth width, w_{st} (mm)	1.6*τ_m/4
Stator teeth yoke width, w_{sty} (mm)	2*τ_m/4
Stator tooth height, h_{st} (mm)	10
Stator yoke height, h_{sy} (mm)	13
Stator height, h_s (mm)	23
Coil spacing, λ_1 (mm)	(2+1/2)*τ_s
Phase spacing, λ_2 (mm)	(5+1/3)*τ_s
Number of turns per coil, N_{coil}	114
Phase resistance (Ω), R_s	3
Stack factor	0.95
Rate current I_{rms} (A)	3
Rated speed (m/s)	1.2
Maximum load (N)	150

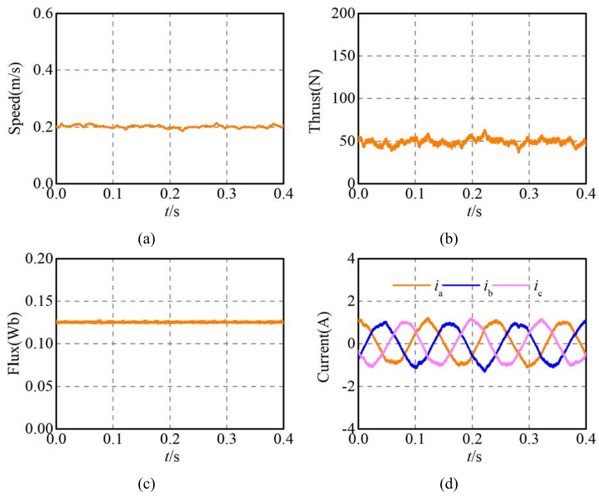

FIGURE 12. Steady-state experiment performance of T-DTFC: (a) speed, (b) thrust, (c) flux (d) phase current.

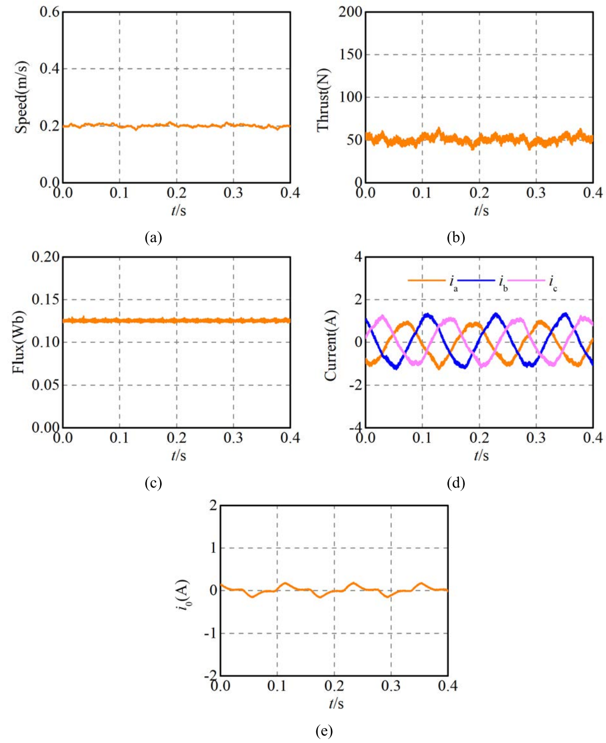

FIGURE 13. Steady-state experiment performance of P-DTFC: (a) speed, (b) thrust, (c) flux (d) phase current, (e) zero sequence current.

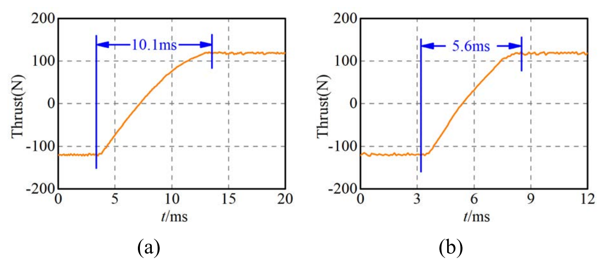

FIGURE 14. The response of thrust force of experiment: (a) T-DTFC, (b) P-DTFC.

V. EXPERIMENTAL VALIDATION

In order to verify the practicability and accuracy of P-DTFC, the HOWEM system is operated based on dSPACE DS1103 controller, as shown in Figure 11. The DC-link voltage is 50 V and the sampling period is 50 ms. The PPMLM parameters are shown in Table 4. The steady-state and dynamic-state experiments of P-DTFC are carried out. In addition, several experiments for T-DTFC are also implemented as a comparison.

A. STEADY-STATE PERFORMANCE OF EXPERIMENT

This experiment is to verify the steady-state performance of the P-DTFC and the T-DTFC. The reference speed is set as 0.2 m/s and the load is 50 N. The experimental results are shown in Figure 12 and Figure 13.

As can be seen from Figure 12 and Figure 13 that the speed is fluctuated around at 0.2 m/s and the thrust force is equal to 50 N approximately in both DTFC since the friction coefficient between mover and stator is variable in different location. The flux linkage is always maintain the constant for each DTFC. Furthermore, a small zero sequence current is existed in P-DTFC, which is caused by the temperature drift effect of the sampling circuit and the zero sequence voltage other than the common mode voltage.

B. THRUST RESPONSE OF EXPERIMENT

In order to compare the thrust response performance of the P-DTFC and the T-DTFC, the reference thrust force increases from −120 N to 120 N, in which the effect of speed regulator is removed. The experimental results are demonstrated in Figure 14.

It can be found that the thrust force response of T-DTFC and P-DTFC is 10.1 ms and 5.6 ms respectively. Since utilization of DC-link voltage is greatly increased, P-DTFC

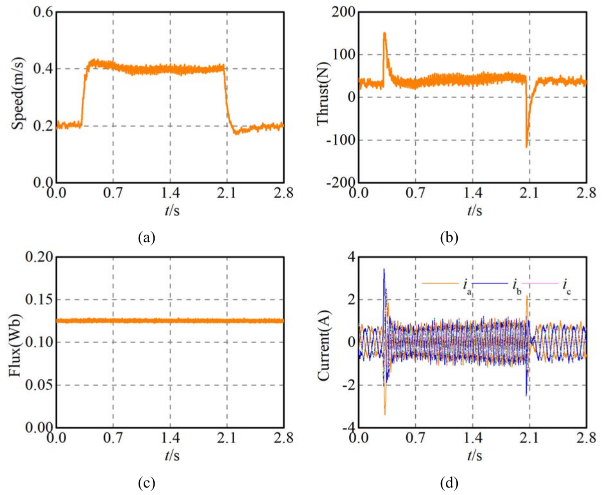

FIGURE 15. Speed response experiment performance of T-DTFC: (a) speed, (b) thrust, (c) flux (d) phase current.

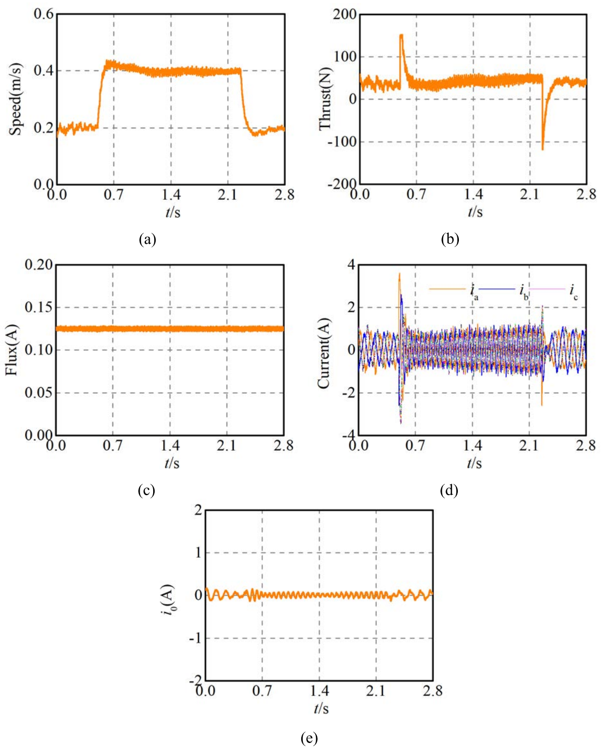

FIGURE 16. Speed response experiment performance of P-DTFC: (a) speed, (b) thrust, (c) flux (d) phase current, (e) zero sequence current.

demonstrates better dynamic performance than that of T_DTFC.

C. SPEED RESPONSE OF EXPERIMENT

This experiment is to verify the speed response of the P-DTFC and the T-DTFC. The reference speed increases from 0.2 m/s to 0.4 m/s, then decreases to 0.2 m/s. The experimental results are illustrated in Figure 15 and Figure 16.

Both P-DTFC and T-DTFC demonstrate good speed response performance. The flux linkage maintains constant value at 0.125 Wb despite of the variable speed. In Figure 15, the zero sequence current is greatly suppressed because of the adoption of IVAV.

VI. CONCLUSION

In this paper, the P-DTFC of HOWEM system is proposed. In order to suppress the zero sequence current, the IVAV is selected as the candidate voltage vector, in which the complexity of control strategies is greatly simplified. Meanwhile, the control voltage vector is selected by a new switch table in P-DTFC. That the P-DTFC maintains better steady-state and dynamic-state performance with lower complexity compared with T-DTFC is verified through the simulation and experimental results.

REFERENCES

[1] W. Wang, W. Tian, Z. Wang, W. Hua, and M. Cheng, "A fault diagnosis method for current sensors of primary permanent-magnet linear motor drives," *IEEE Trans. Power Electron.*, vol. 36, no. 2, pp. 2334–2345, Feb. 2021.

[2] G. Lv, T. Zhou, D. Zeng, and Z. Liu, "Influence of secondary constructions on transverse forces of linear induction motors in curve rails for urban rail transit," *IEEE Trans. Ind. Electron.*, vol. 66, no. 6, pp. 4231–4239, Jun. 2019.

[3] W. Xu, X. Xiao, G. Du, D. Hu, and J. Zou, "Comprehensive efficiency optimization of linear induction motors for urban transit," *IEEE Trans. Veh. Technol.*, vol. 69, no. 1, pp. 131–139, Jan. 2020.

[4] Q. Wang, Y. Chen, Y. Guo, J. Zhang, and Y. Li, "Performance modeling and analysis of a doubly yokeless permanent magnet linear motor with improved thrust force quality," *IEEE Access*, vol. 7, pp. 160586–160594, 2019.

[5] X. Liu, S. Zhen, H. Zhao, H. Sun, and Y.-H. Chen, "Fuzzy-set theory based optimal robust design for position tracking control of permanent magnet linear motor," *IEEE Access*, vol. 7, pp. 153829–153841, 2019.

[6] Y. Sui, Z. Yin, M. Wang, B. Yu, and P. Zheng, "A tubular staggered-teeth transverse-flux PMLM with circumferentially distributed three-phase windings," *IEEE Trans. Ind. Electron.*, vol. 66, no. 6, pp. 4837–4848, Jun. 2019.

[7] X. Yang, W. Zhao, and B. Song, "Thrust force calculation and analysis for the permanent magnet linear motor motion system considering the encoder errors," *IEEE Trans. Ind. Electron.*, vol. 69, no. 6, pp. 6069–6079, Jun. 2022, doi: 10.1109/TIE.2021.3088370.

[8] R. Cao, M. Cheng, and W. Hua, "Investigation and general design principle of a new series of complementary and modular linear FSPM motors," *IEEE Trans. Ind. Electron.*, vol. 60, no. 12, pp. 5436–5446, Dec. 2013, doi: 10.1109/TIE.2012.2230605.

[9] W. Wang, Z. Lu, W. Tian, W. Hua, Z. Wang, and M. Cheng, "Dual-vector located model predictive control with single DC-link current sensor for permanent-magnet linear motor drives," *IEEE Trans. Power Electron.*, vol. 36, no. 12, pp. 14142–14154, Dec. 2021.

[10] Y. Zhong, H. Lin, Z. Chen, S. Lyu, and H. Yang, "Online-parameter-estimation-based control strategy combining MTPA and flux-weakening for variable flux memory machines," *IEEE Trans. Power Electron.*, vol. 37, no. 4, pp. 4080–4090, Apr. 2022, doi: 10.1109/TPEL.2021.3126581.

[11] Z. Hao, Y. Tian, Y. Yang, Y. Gong, Z. Hao, C. Zhang, H. Song, and J. Zhang, "An adaptive angle error compensator for IPMSMs with periodic loads in the flux weakening region," *IEEE Trans. Power Electron.*, vol. 37, no. 4, pp. 4484–4496, Apr. 2022, doi: 10.1109/TPEL.2021.3125951.

[12] W. Zhao, B. Wu, Q. Chen, and J. Zhu, "Fault-tolerant direct thrust force control for a dual inverter fed open-end winding linear Vernier permanent-magnet motor using improved SVPWM," *IEEE Trans. Ind. Electron.*, vol. 65, no. 9, pp. 7458–7467, Sep. 2018.

[13] W. Hu, H. Nian, and D. Sun, "Zero-sequence current suppression strategy with reduced switching frequency for open-end winding PMSM drives with common DC BUS," *IEEE Trans. Ind. Electron.*, vol. 66, no. 10, pp. 7613–7623, Oct. 2019.

[14] L. Rovere, G. Valente, A. Formentini, and P. Zanchetta, "Parameters and volt–ampere ratings of a floating capacitor open-end winding synchronous motor drive for extended CPSR," *IEEE Trans. Ind. Electron.*, vol. 69, no. 5, pp. 4576–4586, May 2022, doi: 10.1109/TIE.2021.3076917.

[15] W. Wang, Y. Jiang, L. Sun, Z. Wang, W. Hua, and M. Cheng, "Phase model predictive voltage control for half-centralized open-end winding permanent-magnet linear motor traction systems," *IEEE Trans. Ind. Electron.*, early access, Dec. 2, 2021, doi: 10.1109/TIE.2021.3130329.

[16] X. Yuan, C. Zhang, and S. Zhang, "Torque ripple suppression for open-end winding permanent-magnet synchronous machine drives with predictive current control," *IEEE Trans. Ind. Electron.*, vol. 67, no. 3, pp. 1771–1781, Mar. 2020.

[17] W. Hu, C. Ruan, H. Nian, and D. Sun, "An improved modulation technique with minimum switching actions within one PWM cycle for open-end winding PMSM system with isolated DC bus," *IEEE Trans. Ind. Electron.*, vol. 67, no. 5, pp. 4259–4264, May 2020.

[18] L. Rovere, A. Formentini, G. L. Calzo, P. Zanchetta, and T. Cox, "Zero-sequence voltage elimination for dual-fed common DC-link open-end winding PMSM high-speed starter–generator—Part I: Modulation," *IEEE Trans. Ind. Appl.*, vol. 55, no. 6, pp. 7804–7812, Nov. 2019.

[19] Z. Shen, D. Jiang, L. Zhu, Y. Xu, T. Zou, Z. Liu, and R. Qu, "A novel zero-sequence current elimination PWM scheme for an open-winding PMSM with common DC bus," *IEEE Trans. Power Electron.*, vol. 34, no. 12, pp. 12476–12490, Dec. 2019, doi: 10.1109/TPEL.2019.2906975.

[20] W. Hu, C. Ruan, H. Nian, and D. Sun, "Zero-sequence current suppression strategy with common-mode voltage control for open-end winding PMSM drives with common DC bus," *IEEE Trans. Ind. Electron.*, vol. 68, no. 6, pp. 4691–4702, Jun. 2021, doi: 10.1109/TIE.2020.2988221.

[21] H. Zhan, Z.-Q. Zhu, and M. Odavic, "Analysis and suppression of zero sequence circulating current in open winding PMSM drives with common DC bus," *IEEE Trans. Ind. Appl.*, vol. 53, no. 4, pp. 3609–3620, Jul. 2017.

[22] M. R. Baiju, K. K. Mohapatra, R. S. Kanchan, and K. Gopakumar, "A dual two-level inverter scheme with common mode voltage elimination for an induction motor drive," *IEEE Trans. Power Electron.*, vol. 19, no. 3, pp. 794–805, May 2004.

[23] V. T. Somasekhar, S. Srinivas, and K. K. Kumar, "Effect of zero-vector placement in a dual-inverter fed open-end winding induction motor drive with alternate sub-hexagonal center PWM switching scheme," *IEEE Trans. Power Electron.*, vol. 23, no. 3, pp. 1584–1591, May 2008.

[24] Y. Zhou and H. Nian, "Zero-sequence current suppression strategy of open-winding PMSG system with common DC bus based on zero vector redistribution," *IEEE Trans. Ind. Electron.*, vol. 62, no. 6, pp. 3399–3408, Jun. 2015.

[25] X. Yuan, S. Zhang, C. Zhang, M. Degano, G. Buticchi, and A. Galassini, "Improved finite-state model predictive current control with zero-sequence current suppression for OEW-SPMSM drives," *IEEE Trans. Power Electron.*, vol. 35, no. 5, pp. 4996–5006, May 2020, doi: 10.1109/TPEL.2019.2942156.

[26] W. Hu, H. Nian, and T. Zheng, "Torque ripple suppression method with reduced switching frequency for open-winding PMSM drives with common DC bus," *IEEE Trans. Ind. Electron.*, vol. 66, no. 1, pp. 674–684, Jan. 2019.

[27] X. Zhang and K. Wang, "Current prediction based zero sequence current suppression strategy for the semicontrolled open-winding PMSM generation system with a common DC bus," *IEEE Trans. Ind. Electron.*, vol. 65, no. 8, pp. 6066–6076, Aug. 2018, doi: 10.1109/TIE.2017.2784353.

[28] Z. Song, S. Hu, Y. Yu, and F. Zhou, "Performance improvement of semi-controlled open-winding PMSGs based on virtual zero-crossing detection and segment injection of third-order harmonic current," *IEEE Trans. Power Electron.*, vol. 34, no. 12, pp. 12050–12063, Dec. 2019, doi: 10.1109/TPEL.2019.2906351.

[29] C. Liu and J. Shang, "Three-dimension space vector based finite control set method for OW-PMSM with zero-sequence current suppression and switching frequency reduction," *IEEE Trans. Power Electron.*, vol. 36, no. 12, pp. 14074–14086, Dec. 2021, doi: 10.1109/TPEL.2021.3087015.

[30] X. Zhang, K. Wang, W. Zhang, Y. Wang, P. Wang, and D. Gao, "Dual delay-compensation-based model predictive control for the semi-controlled open-winding PMSM system," *IEEE Access*, vol. 7, pp. 69947–69959, 2019.

[31] X. Zhang, Y. Li, K. Wang, W. Zhang, and D. Gao, "Model predictive control of the open-winding PMSG system based on three-dimensional reference voltage-vector," *IEEE Trans. Ind. Electron.*, vol. 67, no. 8, pp. 6312–6322, Aug. 2020, doi: 10.1109/TIE.2019.2938478.

[32] X. Lin, W. Huang, W. Jiang, Y. Zhao, D. Dong, and X. Wu, "Direct torque control for three-phase open-end winding PMSM with common DC bus based on duty ratio modulation," *IEEE Trans. Power Electron.*, vol. 35, no. 4, pp. 4216–4232, Apr. 2020, doi: 10.1109/TPEL.2019.2935295.

[33] M. Wang, D. Sun, W. Ke, and H. Nian, "A universal lookup table-based direct torque control for OW-PMSM drives," *IEEE Trans. Power Electron.*, vol. 36, no. 6, pp. 6188–6191, Jun. 2021, doi: 10.1109/TPEL.2020.3037202.

[34] Z. Yu, W. Kong, and R. Qu, "Direct torque control strategy for DC-biased Vernier reluctance machines capable of zero-sequence current regulation," *IEEE Trans. Ind. Electron.*, vol. 68, no. 3, pp. 2024–2033, Mar. 2021, doi: 10.1109/TIE.2020.2977579.

[35] Q. Lu, Y. Zuo, T. Zhang, and L. Mo, "Zero-sequence current suppression for open-winding permanent magnet brushless motor driving system based on second order generalized integrator," *IEEE Access*, vol. 8, pp. 37465–37473, 2020.

[36] Z. Song, X. Ma, and Y. Yu, "Design of zero-sequence current controller for open-end winding PMSMs considering current measurement errors," *IEEE Trans. Power Electron.*, vol. 35, no. 6, pp. 6127–6139, Jun. 2020, doi: 10.1109/TPEL.2019.2952402.

[37] G. Mademlis, N. Sharma, Y. Liu, and J. Tang, "Zero-sequence current reduction technique for electrical machine emulators with DC-coupling by regulating the SVM zero states," *IEEE Trans. Ind. Electron.*, early access, Oct. 21, 2021, doi: 10.1109/TIE.2021.3120485.

[38] Z. Song, S. Hu, and R. Zhang, "Performance improvement of open-winding PMSMs with a discrete-time designed zero-sequence current controller based on virtual three-phase expansion," *IEEE Trans. Ind. Electron.*, vol. 67, no. 12, pp. 10046–10054, Dec. 2020, doi: 10.1109/TIE.2019.2962427.

QIANGGUO YU was born in Hunan, China. He received the B.Sc. degree in electronic information engineering from Hunan University, Changsha, China, in 2000, and the M.Sc. degree in software engineering from Central South University, Changsha, in 2016.

Since 2020, he has been with the Huzhou College, where he is currently a Senior Engineer. His current research interests include intelligent control and pattern recognition.

WEI WANG (Senior Member, IEEE) was born in Jiangsu, China. He received the B.Sc. degree in electrical engineering from the Nanjing University of Science and Technology, Nanjing, China, in 2008, and the Ph.D. degree in electrical engineering from Southeast University, Nanjing, in 2014.

From October 2011 to October 2012, he got the Scholarship from the China Scholarship Council and was a joint Ph.D. Student with the University of Lille 1, Lille, France. Since 2014, he has been with Southeast University, where he is currently an Associate Professor with the School of Electrical Engineering. He is the author or the coauthor of more than 80 technical papers. His research interests include motor drives and traction system for rail transit.

YANAN FENG was born in Anhui, China. He received the B.Sc. degree in electrical engineering from the Anhui University of Technology, Maanshan, China, in 2016, and the M.Sc. degree in electrical engineering from Southeast University, Nanjing, China, in 2019.

Since 2020, he has been with the Huzhou College, Huzhou, China. His current research interest includes control of permanent magnet linear motor.

WEIJIE TIAN (Graduate Student Member, IEEE) was born in Jiangsu, China. He received the B.Sc. degree in electrical engineering from the Shenyang University of Technology, Shenyang, China, in 2018. He is currently pursuing the Ph.D. degree in electrical engineering with Southeast University, Nanjing.

His current research interests include fault diagnosis and control of electrical machine drive systems.

QING SHEN was born in Shanxi, China, in 1982. She received the B.S. degree in computer science and technology and the M.S. degree in computer applications technology from the North University of China, in 2004 and 2007, respectively.

She is currently an Associate Professor with the Huzhou College, Huzhou, China. She is the author or the coauthor of more than 30 articles in refereed international journals. Her current research interests include intelligent information processing and swarm intelligence.